

Nanoscale

Accepted Manuscript



This is an *Accepted Manuscript*, which has been through the Royal Society of Chemistry peer review process and has been accepted for publication.

Accepted Manuscripts are published online shortly after acceptance, before technical editing, formatting and proof reading. Using this free service, authors can make their results available to the community, in citable form, before we publish the edited article. We will replace this *Accepted Manuscript* with the edited and formatted *Advance Article* as soon as it is available.

You can find more information about *Accepted Manuscripts* in the [Information for Authors](#).

Please note that technical editing may introduce minor changes to the text and/or graphics, which may alter content. The journal's standard [Terms & Conditions](#) and the [Ethical guidelines](#) still apply. In no event shall the Royal Society of Chemistry be held responsible for any errors or omissions in this *Accepted Manuscript* or any consequences arising from the use of any information it contains.

ARTICLE

Molecular force transfer mechanisms in graphene oxide paper evaluated using atomic force microscopy and *in situ* synchrotron micro FT-IR spectroscopy

Cite this: DOI: 10.1039/x0xx00000x

Received 00th June 2014,
Accepted 00th January 2014

DOI: 10.1039/x0xx00000x

www.rsc.org/Congwei Wang,^a Mark D. Frogley,^b Gianfelice Cinque,^b Lu-Qi Liu,^c and Asa H. Barber^{a,*}

The mechanical properties of graphene oxide (GO) paper are critically defined both by the mechanical properties of the constituent GO sheets and the interaction between these sheets. Functional carbonyl and carboxyl groups decorating defects, expected to be predominantly sheet edges of the GO, are shown to transfer forces to the in-plane carbon-carbon bonding using a novel technique combining atomic force microscopy (AFM) to mechanically deform discrete volumes of GO materials while synchrotron Fourier-transform infra-red (FTIR) microspectroscopy evaluated molecular level bond deformation mechanisms of the GO. Spectroscopic absorption peaks corresponding to in-plane aromatic C=C bonds from GO sheets were observed to shift during tensile tests. Importantly, FTIR provided information on clear absorption peak shifts from C=O bonds linking along the GO sheet edges, indicating transfer of forces between both C=C and C=O bonds during tensile deformation. Grüneisen parameters were used to quantitatively link the macroscopic FTIR peak shifts to molecular level chemical bond strains, with relatively low bond strains prevalent when applying external forces to the GO paper suggesting probing of hydrogen bonding interactions. We propose a mechanistic description of molecular interactions between GO sheets in the paper from these experiments, which is important in future strategies for further modification and improvement of GO-based materials.

Introduction

Graphene oxide (GO) is an increasingly important material used for scalable, cost-effective routes to fabricate graphene devices¹⁻³ and is typically produced by solution-based chemical modification of graphite^{4,6}. Resultant GO retains the 2D planar structure of graphene but is also additionally decorated with functional groups, such as hydroxyl, carboxyl and carbonyl groups along the basal plane and edges¹⁻⁶. This unique structure causes graphene oxide to self-assemble into a hierarchical paper-like material⁷⁻¹⁰ that shows promise in flexible electrodes¹⁰, mechanical actuators¹¹, novel energy generators¹²⁻¹⁴ and high-performance composites¹⁵. The mechanical properties of the GO paper are critical in these applications and superior to similar layered sheet-like structures such as bucky paper¹⁶ and vermiculite¹⁷. Overall mechanical properties of the GO paper are defined by the mechanical behavior of the individual GO sheets, dictated by the sp²-hybridized bonds as

well as the density of defects and functional groups in the GO sheets, the organization of the sheets and, critically, the efficiency of force transfer between the GO sheets in the paper. Therefore, a comprehensive understanding of deformation mechanisms of GO paper and the force transfer between sheets is important for optimizing the mechanics of GO paper for further applications.

Previous studies have examined the mechanical properties of GO paper using conventional macroscopic mechanical testing methods and applied composite theory to consider the papers as reinforcing GO sheets with a stress transfer element defined by the functional groups decorating the sheets⁷⁻⁹. Further understanding of the deformation mechanisms in GO paper has considered micro-structure and, specifically, crosslinks between GO sheets in the paper¹⁸⁻²⁰ using computational simulations to increase the crosslink interaction to give increases in the elastic modulus of the GO paper^{19, 20}. Many of these crosslinks were based on the presence of water-assisted hydrogen bonding

between the GO sheets. However, few direct experimental works have attempted to consider the molecular level deformation mechanisms at both the GO sheets and the interfacial region between the sheets during external loading. Recent progress in experimental mechanics has been used to deform discrete volumes of GO, isolated using focused ion beam (FIB) microscopy, to failure using atomic force microscopy (AFM)²¹. This work applied strategies previously developed for determining specific component mechanics in multi-phase systems, including individual nanofibers in bone²² and simple composite volumes in mineralized tissues²³, and is considered advantageous for understanding inherent GO paper behavior as relatively small samples prepared using FIB are devoid of large defects present when testing at the macroscale. However, AFM mechanical testing of GO paper at small length scales currently lacks the structural information previously examined in computer simulations despite having sufficient force resolution to determine molecular mechanisms.

We attempt to describe the deformation behavior of GO paper by mechanically testing discrete volumes of GO while recording structural changes at the molecular scale. Raman spectroscopy has been previously highlighted as providing such structural information for graphene materials including determination of the number of layers²⁴, the doping quality²⁵ and probing defects edges²⁶ but is limited in GO studies where many of the functional groups i.e. hydroxyl, carboxyl and carbonyl groups weakly scatter in Raman spectroscopy. In this work, we exploit FTIR microspectroscopy to provide molecular level deformation information for GO paper, especially as many of these chemical functionalities in GO are strongly identifiable in IR spectroscopy. As the inherent properties of the GO requires mechanical testing of relatively small volumes, *in situ* FTIR synchrotron microspectroscopy is exploited to give unprecedented corresponding molecular level deformation information within this small volume.

Results and discussion

The inherent properties of GO material were investigated by first isolating GO micro-beams from dense void-free regions of the GO paper using FIB. Mechanical deformation was then applied to the FIB-fabricated micro-beams using AFM. Fig. 1 schematically shows the experimental setup with the orientation of the GO micro-beam relatively to the AFM and synchrotron IR beam used to apply force and provide molecular information respectively. The AFM provided mechanical deformation of the micro-beam along the horizontal axis whereas the IR beam was incident normal to the paper plane and polarized along the strain axis to give structural information within the micro-beam along the deformation direction.

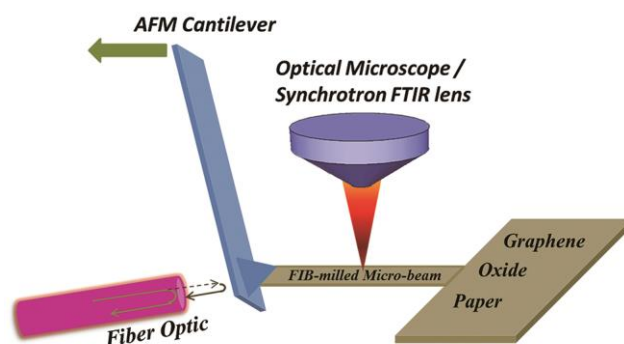


Fig. 1 Schematic diagram showing the experimental setup incorporating AFM for mechanical testing of an individual FIB-milled GO micro-beam and structural evaluation using synchrotron FTIR.

Fig. 2 shows optical images of an individual GO micro-beam tensile tested to failure. We note that the sample failure was towards the middle of the micro-beam as defined for a successful test.

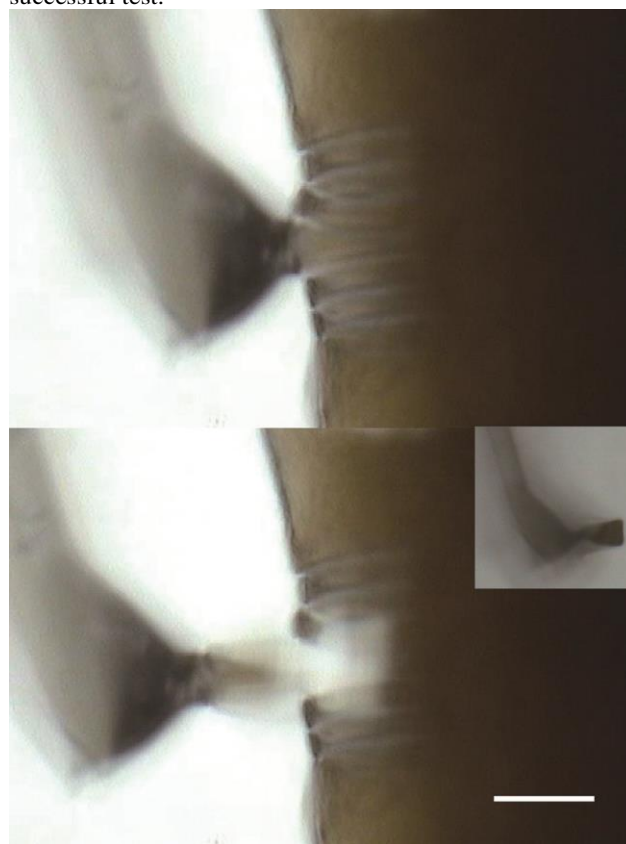


Fig. 2 Optical images showing an individual GO micro-beam before (top) and after (bottom) tensile testing, with the inset showing the failed GO fragment attached to the AFM tip (scale bar is 20 μm).

A typical FTIR absorbance spectrum in transmission for an individual GO micro-beam is shown in Fig. 3a at the start of the mechanical testing step. The absorption peaks in the spectrum can be readily identified and corresponds to a range of chemical bonds¹⁸ including edge carbonyls and carboxyls C=O, COOH ($1500\text{-}1900\text{cm}^{-1}$), sp^2 -hybridized aromatic in-plane C=C ($\sim 1500\text{-}1600\text{cm}^{-1}$), epoxides C-O-C ($\sim 1250\text{-}1350\text{cm}^{-1}$ and

$\sim 850\text{ cm}^{-1}$) and hydroxyls groups, C-OH, COOH, H₂O ($>3000\text{ cm}^{-1}$), which provided evidence of the decoration of functional groups in the GO sheets and trapped water between the GO sheets. Critically, the C=C and C=O absorption peaks were relatively sharp and distinctive within spectra, and were therefore monitored during deformation of the GO micro-beams.

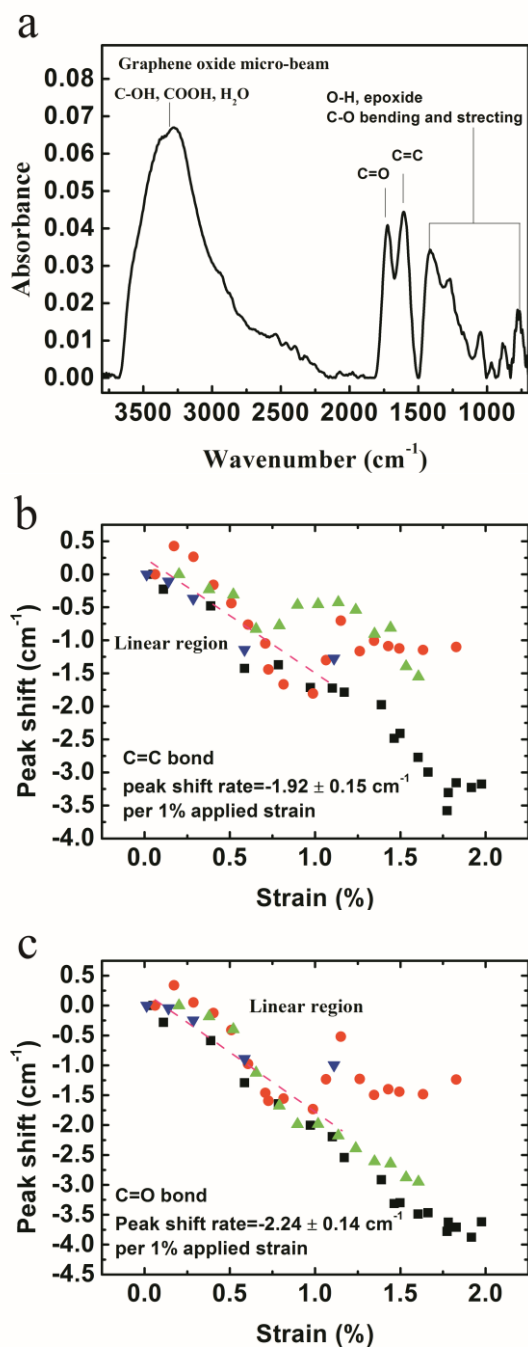


Fig. 3 (a) FTIR spectrum for an individual GO paper micro-beam at zero applied strain. (b) C=C bond peak shift with applied strain, the dash line showing the linear fitting of bond peak shifting rate with applied strain. (c) C=O bond peak shift with applied strain.

Four individual GO paper micro-beam samples were successfully tensile tested while recording the IR spectra during loading, denoted using four different coloured data sets as shown in Fig. 3b, 3c and 5. Fig. 3b shows the C=C bond peak shift with applied strain for the GO micro-beam samples. The plot shows the peak shifting to lower wavenumbers, indicated by a negative peak shift, with applied strain. This downward shift is expected for the aromatic C=C bond under the applied strain due to the elongation of bond distance. Similar downshifts for in-plane C=C bonds have been observed in single layer graphene²⁷⁻²⁹ and GO paper⁸ by Raman spectroscopy. The C=C peak shift was observed, in some cases, to plateau with applied strain. This observation is indicative of a lack of force transfer to the GO sheets with applied strain due to probable failure of the interaction between GO sheets that causes subsequent sliding of sheets over one another. The interaction between GO sheets appears to be variable as the applied strain provided a linear peak shift ranging from 1-2%. Fluctuations in the peak shift with strain, which is particularly apparent in Fig. 3b, are expected to be due to the irregular microstructures within the GO paper micro-beam. Least-squares estimation of the linear region was used to quantitatively calculate the peak shifting rate of this bond red-shift, which gives a C=C bond peak shifting rate of $-1.92 \pm 0.15\text{ cm}^{-1}/1\%$ applied strain. This shifting rate is comparable to C=C bond peak shifting observations made using Raman spectroscopy²⁷⁻²⁹. Fig. 3c shows an additional C=O bond peak shift found in GO with applied strain. The C=O peak shift with applied strain appears to show a more consistent behavior, suggesting homogeneous deformation across all samples, when compared to the C=C bond shifts in Fig. 3b. Linear fitting was again used to provide a C=O bond peak shift of $-2.24 \pm 0.14\text{ cm}^{-1}/1\%$ applied strain.

Peak shifts with applied strain are indicative of structural changes occurring in the GO micro-beams during mechanical deformation. The position of absorption peaks in the FTIR spectrum represent the vibrational energy of chemical bonds in systems, with shifts of absorption peaks representing the vibrational energy changes in chemical bonds. For mechanical testing, this energy change is the result of external applied strain, which provides extra mechanical energy to the chemical bonds. The strain in bonds from consideration of vibrational energy is described by Grüneisen parameters, which evaluates the relationship between volume changes in a crystal lattice and resultant vibrational properties of the lattice. Specifically, the magnitude of a bond peak shift with applied strain is proportional to a Grüneisen parameter. Therefore the introduction of Grüneisen parameters is able to link the measured bond peak shift to chemical bond strain. Such an approach has been previously used to study the uniaxial strain in single layer graphene by Raman spectroscopy³⁰. The measured absorption peak shift for the GO micro-beams is linked to the microscopic bond strain under uniaxial tensile stress. Resultant peak shifts are due to bond deformation along the external force direction and can be described using Equation (1)³⁰:

$$\begin{aligned} \Delta\omega &= -\omega^0\gamma(1-\nu)\varepsilon_L - \frac{1}{2}\beta\omega^0(1+\nu)\varepsilon_L \\ &= \omega^0\varepsilon_L \left[-\gamma(1-\nu) - \frac{1}{2}\beta(1+\nu) \right] \end{aligned} \quad (1)$$

where $\Delta\omega$ is the FTIR peak shift, ω^0 is the FTIR peak position at zero strain, ν is Poisson's ratio of the GO and Grüneisen parameters linking phonon frequencies to lattice strain stated as $\gamma = 1.99$ and $\beta = 0.99$ from measurements in single layer graphene³⁰. We note that ε_L in Equation (1) represents the GO lattice strain. However, the FTIR is polarized and probes C=C bonds along the strain axis only. The GO lattice strain can be linked to the C=C bond strain with a simplified geometrical model considering the lattice geometries and orientations. A schematic graph showing the GO lattice orientations along the external strain axis is shown in Fig. 4.

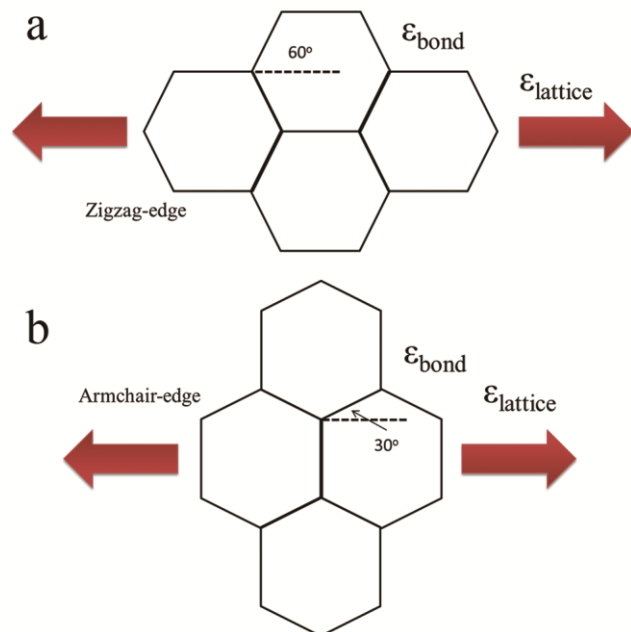


Fig. 4 Schematic of the lattice orientations along the external load, (a) zigzag-edge lattice orientation and (b) armchair-edge lattice orientation. Orientation is determined by the edge type perpendicular to the external load.

Two lattice orientations have been considered in this figure and three simplified conditions assumed for linking the lattice strain with C=C bond strain. Firstly, the basal plane of GO sheet retains the 2D structure of graphene, which mostly consists of sp^2 bonded carbon atoms and no structural distortions brought by the functional groups. Secondly, two typical lattice orientations were considered with an equal distribution between these two lattice orientations. Finally, the lattice is considered to be under small strain during external loading, resulting in equal bond strain for the six carbon atoms in each hexagonal ring of the GO paper. Therefore, for a zigzag-edge lattice orientation as shown in Fig. 4a, two equivalent C=C bonds lie parallel to the external load, whereas four equivalent C=C bonds contribute to the lattice strain at a 60° angle to the loading direction. The relationship between zigzag-edge lattice strain and C=C bond strain can be written as:

$$\varepsilon_{zigzag} = \frac{2}{6}\varepsilon_{bond} + \frac{4}{6}\varepsilon_{bond} \cos 60^\circ = \frac{2}{3}\varepsilon_{bond} \quad (2)$$

Similarly, for an armchair-edge lattice orientation as shown in Fig. 4b, two equivalent C=C bonds are perpendicular to the external load and do not contribute to the overall lattice strain. Four C=C bonds thus contribute equivalently to the lattice

strain at an angle of 30° to the loading direction. The relationship between armchair lattice strain and C=C bond strain can be written as:

$$\varepsilon_{armchair} = \frac{4}{6}\varepsilon_{bond} \cos 30^\circ = \frac{\sqrt{3}}{3}\varepsilon_{bond} \quad (3)$$

Since the GO paper is assumed to contain an equal distribution of zig-zag and armchair lattice orientations, the relationship between GO lattice strain and C=C bond strain is given as:

$$\varepsilon_{lattice} = f_1\varepsilon_{armchair} + f_2\varepsilon_{zigzag} = \frac{1}{2}\varepsilon_{armchair} + \frac{1}{2}\varepsilon_{zigzag} = 0.622\varepsilon_{bond} \quad (4)$$

where f_1 and f_2 are the portion of the two lattice orientations in GO. Substituting lattice strain with C=C bond strain thus provides:

$$\Delta\omega = 0.622\omega^0\varepsilon_B \left[-\gamma(1-\nu) - \frac{1}{2}\beta(1+\nu) \right] = -1.43\omega^0\varepsilon_B \quad (5)$$

The molecular strain (ε_B) of the C=C chemical bond can therefore be determined by knowing the bond peak position at zero strain and solving Equation (5).

The C=C bond peak shifting rate with bond strain is calculated by substituting the bond peak position at zero strain and the peak shift with applied strain for each test into Equation (5). The linear region within Fig. 3b shows the C=C peak shift with applied strain and provides a calculated C=C peak shift with bond strain of $-22.97 \pm 0.33 \text{ cm}^{-1}/1\%$ bond strain. This peak shift with C=C bond strain measured using the FTIR in our work is comparable to previous literature using Raman spectroscopy²⁷⁻²⁹. A resultant plot of C=C bond strain, calculated using Equation (5), against applied strain is shown in Fig. 5.

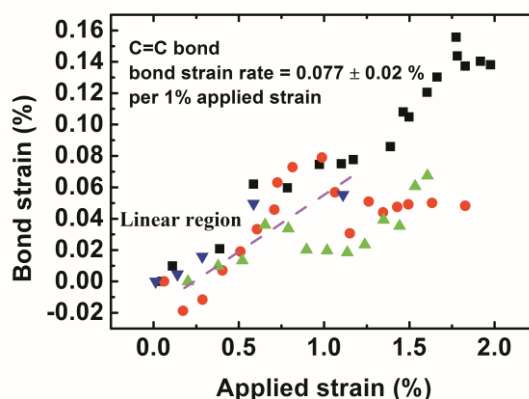


Fig. 5 Plot of C=C bond strain with applied strain. The fit line shows the least-square estimation of bond strain rate with applied strain.

The C=C bond strain is observed to be significantly less than the applied strain in the figure, with a C=C bond strain of $0.077 \pm 0.02\% / 1\%$ applied strain by linear fitting of the data in Fig. 5. This inefficient strain transfer to the GO sheets that provides a small C=C bond strain with applied strain suggests a further phase is straining considerably during sample deformation.

Therefore, examination of the edge linking carbonyls C=O bonds is required to understand the origin of the deformation mechanism within the paper. Previous studies^{2-4, 8} have shown that oxidation of GO causes decoration of the GO sheets with carboxyl and carbonyl groups. These carboxyl and carbonyl groups functional groups at adjacent GO sheets present opportunities for crosslinking through hydrogen bonding^{8, 9, 18, 19}. Due to the directional filtration process, GO sheets consisting of C=C bonds are mostly aligned perpendicular to the filtration direction whereas C=O bonds in carboxylic acids will be oriented at an angle θ relative to the C=C bonds. We therefore propose a mechanism to describe the transfer of forces and resultant bond strains within the GO paper. Spring model for chemical bonds have been introduced for investigating the atomic interactions and elastic properties of single molecule³¹, hydrogen bonding involved IR absorption³² and bond formation and interaction in cells or nanoparticles³³. A simplified spring model can be presented as shown in Fig. 6 to illustrate the interaction between C=C bond and C=O bond. The model assumes a complete dispersion of GO sheets within the paper. Clusters of unexfoliated GO sheets will provide poorer stress transfer within the clusters, causing smaller C=C and C=O peak shifts with applied strain. However, considerable exfoliation of the GO sheets was achieved to form the GO paper (see Electronic Supplementary Information), suggesting the model is approximately valid for experimental conditions.

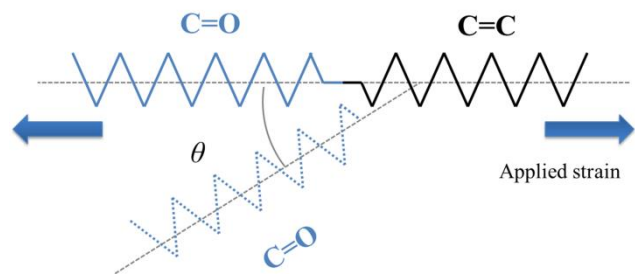


Fig. 6 Schematic showing the coupling of a C=C bond with a C=O bond oriented at an angle θ to the externally applied force.

Specifically, C=C and C=O bonds are stated as two springs connected in series along the direction parallel to the applied external force. Hookean behavior can be considered for the C=C and C=O bonds to provide a relationship (see derivation in Electronic Supplementary Information) between the chemical bond strain rate with applied strain, the force constants for chemical bonds and the resultant bond angle as:

$$\frac{d\varepsilon_{C=O}}{d\varepsilon_{\text{applied}}} = f(\cos\theta) = \frac{k_{C=C}}{k_{C=O}} \frac{d\varepsilon_{C=C}}{d\varepsilon_{\text{applied}}} \frac{1}{\cos\theta} \quad (6)$$

where $k_{C=C}$ and $k_{C=O}$ are the force constants for C=C and C=O bond types and $\Delta\varepsilon_{C=C}$ and $\Delta\varepsilon_{C=O}$ are the corresponding bond strains. The ratio of force constants for C=C and C=O bonds can be extracted in Equation (6) by knowing the peak positions of these two bonds from IR microspectroscopy. Stiffer chemical bonds in a stretching vibrational mode will therefore appear at higher wavenumbers in IR microspectroscopy. The C=C bond strain with applied strain is used to define the relationship between C=O bond strain with applied strain as a function of the relative bond angle using Equation (6). We note that our quasi-static considerations assume the C=C and C=O bonds examined in this work behaves as purely elastic springs.

However, viscoelastic response from other components, such as interfacial regions, may provide time-dependent behaviour in potential dynamic loading conditions and result in variations in the stress transfer to bonds considered.

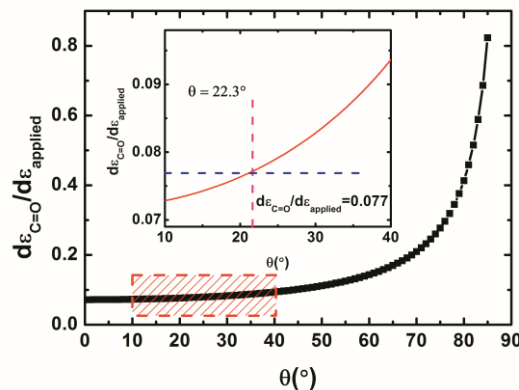


Fig. 7 Relationship between C=O bond strain per applied strain with relative angle between the C=C and C=O bonds. Insert shows the magnified region from 10° to 40°.

Fig. 7 shows the average relationship between C=O bond strain with the applied strain against a range of C=C/C=O bond angles calculated using Equation (6) for all experimental data. The change of C=O bond strain rate is shown to increase with the bond angle and exhibits non-linear behavior. For C=C and C=O bonds in series, i.e. $\theta = 0^\circ$, the strain rate in the C=O bond with applied strain is smallest. Increases in the C=O angle relative to the C=C bond, which is assumed to lie in the direction of the loading axis, require an increased rate of C=O bond strain with applied strain. The plot in Fig. 7 also highlights the interaction between the C=C and C=O bonds with lower and higher force constant respectively. Specifically, the insert in Fig. 7 shows the condition when the rate of C=O bond strain is equal to the previous rate of C=C bond strain at a bond angle of 22°. For bond angles below 22°, the C=O bond is stiffer than the C=C bond and therefore displays a lower bond strain with applied strain as highlighted in the figure, which is physically reasonable. A larger misalignment of C=O bonds relative to the C=C bonds thus cause larger bond strains in the C=O bonds despite their force constants being larger. Experimentally, the C=O absorption peak is previously observed in Fig. 3b as occurring at a higher wavenumber than the C=C peak and indicates an expected higher force constant. The increased wavenumber shift with applied strain shown for the C=O band relative to the C=C further indicates that this stiffer C=O bond is also straining more than that of the C=C bond with applied strain. We can thus conclude that a higher rate of C=O bond strain compared to C=C bond strain can only occur if the C=O bonds are position at angles greater than 22° to the C=C bonds in the graphene oxide paper. C=O IR absorption peak widths and heights are also found to change little with applied external strain (see Electronic Supplementary Information), which suggests that the linking bonding structures between the sheets show little reorientation and alignment during mechanical loading. The proposed orientation of the out of plane C=O functional groups indicated in Fig. 7 corroborates previous modelling work^{19,20}, although authors of these works did not

comment on the significance of this structure such as in the transfer of stress as shown in this current paper.

Conclusions

In summary, molecular level deformation mechanisms in GO paper were evaluated using novel experimental techniques combining AFM, which provided tensile deformation of the sample, and synchrotron-FTIR microspectroscopy to probe resultant bond strain. Results highlighted the interaction between in-plane C=C and cross-linking C=O bonds within the GO paper from probing corresponding absorption band shifts with applied strain. Investigations were able to provide evidence of weak bonding between the sheet structures in GO paper and interestingly elucidated relatively large C=O peak shift with applied strain. A bond organization model emphasized the requirement for C=O bonds to be aligned at least 22° out of plane in order to satisfy the observed experimental data. The improvement of GO paper mechanics therefore requires enhancement in the force transferred between the C=C and C=O bonds evaluated in this work so that larger C=C and C=O peaks shifts with external straining are achieved. This novel combination of AFM and synchrotron micro FT-IR spectroscopy also provides opportunities to investigate mechanical behaviour of a range of materials while monitoring changes of IR active chemical bonds *in situ*, which is important for understanding structure-mechanical property relationships in deformed synthetic fibres³⁴ and composite materials³⁵ that contain strain sensitive IR active functional chemical bonds.

Experimental Section

Preparation of graphene oxide and GO paper

GO sheets were synthesized by the modified Hummer's method followed by mechanical exfoliation with the assistance of sonication⁸. Specifically, Graphite flakes were obtained from Alfa Aesar Co. Ltd. (U. K.), with a listed graphite flake average size of 325 mesh, corresponding to 44 µm. All other reagents were purchased from Sigma-Aldrich (U. K.). A 2 g portion of natural flake graphite and 2 g of NaNO₃ were mixed with 96 mL of concentrated H₂SO₄ (98 wt. %) in an ice bath. The mixture was continuously stirred using a magnet stirrer while 10 g of KMnO₄ was gradually added to prevent the temperature from exceeding 5 °C. The mixture obtained was first stirred at 0 °C for 90 min and then at 35 °C for 2 h. Distilled water (80 mL) was subsequently dropped slowly into the resulting solution to dilute the mixture. 200 mL of distilled water was further added followed by 15 mL of H₂O₂ (30 wt. %), and the stirring continued for 10 min to obtain a bright-yellow graphite oxide suspension. The graphite oxide suspension was centrifuged and carefully washing in 5 wt. % HCl and deionized water to remove remnant salt. Colloidal dispersions of GO were exfoliated using an ultrasonic cleaner. GO paper was produced by filtration of the resulting colloid through a cellulose membrane filter (47 mm in diameter, 0.22 µm pore size), followed by air drying.

Fabrication of GO paper micro-beams

A piece of as-synthesized GO paper with dimensions of approximately 15 mm x 3 mm x 0.012 mm was cut from the collected paper using a sharp blade. Discrete volumes of GO free from local defects such as large voids and less-densely stacked regions as observed using scanning electron

microscopy (SEM) were selected using FIB assisted milling to cut the GO paper into micro-beams. Micro-beam production was carried out using previous FIB milling strategies²². A FIB current of 0.1 nA and an accelerating voltage above 15 kV was used to fabricate micro-beams samples free from ion beam-induced damage, as previously reported³⁶.

In situ AFM mechanical tensile test

Isolated GO paper micro-beams were mechanically tested in air using a custom build AFM (Attocube GmbH, Ger.) that allows top-down optical access³⁷. This setup essentially used an AFM orientated 90° along its horizontal axis and was situated under an *in situ* synchrotron FTIR (B22 beamline, Diamond Light Source, U.K.) that evaluated structural changes in the GO paper. Mechanical testing was performed as previously reported^{21, 23} by first placing an uncured droplet of epoxy glue (Poxipol, Arg.) approximately 1-2 mm in diameter at the edge of the AFM sample stage. A FIB flattened AFM tip was first translated into contact with the glue droplet and removed using the AFM xyz piezo-positioners in order to deposit glue at the AFM tip apex. Subsequently, the AFM tip was moved into contact with the free end of the milled GO paper micro-beam. The glue at the contact point between the AFM tip and free end of the GO paper beam was allowed to cure for at least 90 minutes in air. Attachment of the AFM tip to the sample and subsequent manipulation was monitored in a top-down configuration using an optical microscope (Bruker, Ger.). The GO micro-beam was initially placed into pre-tension before mechanical testing. This pre-tension may cause sample relaxation, especially at initial strains as shown for some of the samples in Fig. 3b and Fig. 3c. Mechanical testing was achieved by translating the AFM tip, attached to the free end of the GO micro-beam, along the long axis of the micro-beam to provide tensile deformation in the sample at a displacement rate of 0.5 µm·min⁻¹. The force applied to the sample was recorded using an interferometer positioned behind the cantilever to measure resultant AFM cantilever deflection. The cantilever deflection was converted to force by knowing the spring constant of the cantilever, calculated using the thermal noise method³⁸. The sample strain (ϵ) was calculated using $\epsilon = (\Delta l/l_0) \times 100\%$, where l_0 is the original micro-beam length and Δl is the micro-beam extension distance. Δl was measured using $\Delta l = D - d$ where D is the AFM piezo movement in the testing axis direction and d is the AFM cantilever deflection. Synchrotron FTIR spectra were recorded *in situ* while the GO micro-beam was tensile tested to failure. The tensile testing was paused at 100 nm piezo movement intervals to record an FTIR spectrum. Two IR apertures of 8 x 8 µm and 10 x 10 µm, both of which were comparable with the width of GO paper micro-beam, were used to record IR spectra. The IR beam was located at the centre of the micro-beam to collect the *in situ* chemical information of the sample during mechanical deformation. A total of 4 GO micro-beam samples were successfully tensile tested while recording the IR spectra during loading to failure. We note that a successful test was when the micro-beam failed towards the middle of its length (Fig. 2) and away from the bulk sample or contact with the AFM tip, with approximately 30% of micro-beams produced successfully failing in the middle of the sample.

Acknowledgements

The authors acknowledge financial support through Diamond AP 12. CW acknowledges support through the Chinese Scholarship Scheme.

Notes and references

^a Department of Materials, School of Engineering and Materials Science, Queen Mary University of London, Mile End Road, London E1 4NS, U. K.

^b Diamond Light Source Ltd., Harwell Science and Innovation Campus, Didcot, OX11 0DE, U. K.

^c National Center for Nanoscience and Technology, China, Beijing 100190, P. R. China.

*To whom correspondence should be addressed: a.h.barber@qmul.ac.uk

† Electronic Supplementary Information (ESI) available: [X-ray diffraction of GO paper; AFM images of fabricated GO sheets; proposed model to describe coupling between C=C and C=O bonds in GO paper and C=O bond peak full width at half maximum and peak intensity during the mechanical testing]. See DOI: 10.1039/b000000x/

- S. Stankovich, D. A. Dikin, G. H. B. Dommett, K. M. Kohlhaas, E. J. Zimney, E. A. Stach, R. D. Piner, S. T. Nguyen and R. S. Ruoff, *Nature*, 2006, **442**, 282.
- S. Park and R. S. Ruoff, *Nat. Nanotechnol.*, 2009, **4**, 217.
- S. Stankovich, D. A. Dikin, R. D. Piner, K. A. Kohlhaas, A. Kleinhammes, Y. Jia, Y. Wu, S. T. Nguyen and R. S. Ruoff, *Carbon*, 2007, **45**(7), 1558
- D. R. Dreyer, S. Park, C. W. Bielawski and R. S. Ruoff, *Chem. Soc. Rev.*, 2010, **39**, 228.
- K. A. Mkhoyan, A. W. Contryman, J. Silcox, D. A. Stewart, G. Eda, C. Mattevi, S. Miller and M. Chhowalla, *Nano Lett.*, 2009, **9**, 1058.
- T. Kuilla, S. Bhadra, D. Yao, N. H. Kim, S. Bose and J. H. Lee, *Prog. Polym. Sci.*, 2010, **35**, 1350.
- D. A. Dikin, S. Stankovich, E. J. Zimney, R. D. Piner, G. H. B. Dommett, G. Evmenenko, S. T. Nguyen and R. S. Ruoff, *Nature*, 2007, **448**, 457.
- Y. Gao, L.-Q. Liu, S.-Z. Zu, K. Peng, D. Zhou, B.-H. Han and Z. Zhang, *ACS Nano*, 2011, **5**, 2134.
- S. Park, K. S. Lee, G. Bozoklu, W. W. Cai, S. T. Nguyen and R. S. Ruoff, *ACS Nano*, 2008, **2**, 572.
- C. Yan, J. H. Cho and J.-H. Ahn, *Nanoscale*, 2012, **4**, 4870.
- H. Q. Chen, M. B. Müller, K. J. Gilmore, G. G. Wallace and D. Li, *Adv. Mater.*, 2008, **20**, 3557.
- T. Kuilla, A. Kumar Mishra, P. Khanra, N. H. Kim and J. H. Lee, *Nanoscale*, 2013, **5**, 52.
- Y. Wang, Z. Shi, Y. Huang, Y. Ma, C. Wang, M. Chen and Y. Chen, *J. Phys. Chem. C*, 2009, **113**, 13103.
- H. Wang, Q. Hao, X. Yang, L. Lu and X. Wang, *Electrochem. Commun.*, 2009, **11**(6), 1158.
- Q. Cheng, M. Wu, M. Li, L. Jiang and Z. Tang, *Angew. Chem., Int. Ed.*, 2013, **52**, 3750.
- X. F. Zhang, T. V. Sreekumar, T. Liu, and S. Kumar, *J. Phys. Chem. B*, 2004, **108**, 16435.
- D. G. H. Ballard and G. R. Rideal, *J. Mater. Sci.* 1983, **18**, 545.
- M. Acik, C. Mattevi, C. Gong, G. Lee, K. Cho, M. Chhowalla and Y. J. Chabal, *ACS Nano*, 2010, **4**, 5861.
- N. V. Medhekar, A. Ramasubramaniam, R. S. Ruoff and V. B. Shenoy, *ACS Nano*, 2010, **4**, 2300.
- O. C. Compton, S. W. Cranford, K. W. Putz, Z. An, L. C. Brinson, M. J. Buehler and S. T. Nguyen, *ACS Nano*, 2012, **6**, 2008.
- C. Wang, M. D. Frogley, G. Cinque, L. Q. Liu and A. H. Barber, *Carbon* 2013, **63**, 471.
- F. Hang and A.H. Barber, *J. R. Soc. Interface* 2011, **8**, 500.
- I. Jimenez-Palomar, A. Shipov, R. Shahar and A.H. Barber, *J. Mech. Beh. Biomed. Mater.* 2012, **5**, 149.
- A. C. Ferrari, J. C. Meyer, V. Scardaci, C. Casiraghi, M. Lazzeri, S. Piscanec, D. Jiang, K. S. Novoselov, S. Roth and A. K. Geim, *Phys. Rev. Lett.*, 2006, **97**, 187401.
- C. Casiraghi, S. Pisana, K. S. Novoselov, A. K. Geim and A. C. Ferrari, *Appl. Phys. Lett.*, 2007, **91**, 233108.
- L. G. Cancado, M. A. Pimenta, B. R. A. Neves, M. S. S. Dantas and A. Jorio, *Phys. Rev. Lett.*, 2004, **93**, 247401.
- Z. H. Ni, T. Yu, Y. H. Lu, Y. Y. Wang, Y. P. Feng and Z. X. Shen, *ACS Nano*, 2008, **2**, 2301.
- F. Ding, H. Ji, Y. Chen, A. Herklotz, K. Dörr, Y. Mei, A. Rastelli and O. G. Schmidt, *Nano Lett.*, 2010, **10**, 3453.
- T. Yu, Z. Ni, C. Du, Y. You, Y. Wang and Z. Shen, *J. Phys. Chem. C*, 2008, **112**, 12602.
- T. M. G. Mohiuddin, A. Lombardo, R. R. Nair, A. Bonetti, G. Savini, R. Jalil, N. Bonini, D. M. Basko, C. Galiotis, N. Marzari, K. S. Novoselov, A. K. Geim and A. C. Ferrari, *Phys. Rev. B: Condens. Matter Mater. Phys.*, 2009, **79**, 205433.
- T. C. Lim, *J. Math. Chem.* 2003, **34**, 215.
- Y. Chen, Y. Cao, Y. Zhang and T. Mu, *J. Mol. Struct.* 2014, **1058**, 244.
- N. W. Moore and T. L. Kuhl, *Biophys. J.*, 2006, **91**, 1675.
- U. Stachewicz, F. Hang, R. J. Bailey, H. S. Gupta, M. D. Frogley, G. Cinque and A. H. Barber, *Mater Res Soc Symp Proc*, 2012, **1424**, 11-1424.
- L. S. Loo and K. K. Gleason, *Macromolecules*, 2003, **36**, 2587.
- R. J. Bailey, R. Reurts, D. J. Stokes, F. de Jong and A. H. Barber, *Micron*, 2013, **50**, 51.
- F. Hang, D. Lu, R. J. Bailey, I. Jimenez-Palomar, U. Stachewicz, B. Cortes-Ballesteros, M. Davies, M. Zech, C. Bödefeld and A. H. Barber, *Nanotechnology*, 2011, **22**, 365708.
- J. E. Sader, J. W. M. Chon and P. Mulvaney, *Rev. Sci. Instrum.* 1999, **70**, 3967.